ARMY RESEARCH LABORATORY

Isotope Generated Electron Density in Silicon Carbide Direct Energy Converters

by Marc Litz and Kara Blaine

ARL-TR-3964 **October 2006**

NOTICES

Disclaimers

The findings in this report are not to be construed as an official Department of the Army position unless so designated by other authorized documents.

Citation of manufacturer's or trade names does not constitute an official endorsement or approval of the use thereof.

Destroy this report when it is no longer needed. Do not return it to the originator.

Army Research Laboratory
Adelphi, MD 20783-1197

ARL-TR-3964 **October 2006**

Isotope Generated Electron Density in Silicon Carbide Direct Energy Converters

Marc Litz and Kara Blaine
Sensors and Electron Devices Directorate, ARL

REPORT DOCUMENTATION PAGE

Form Approved
OMB No. 0704-0188

1. REPORT DATE *(DD-MM-YYYY)*	2. REPORT TYPE	3. DATES COVERED (From - To)
October 2006	Draft	May 2006

4. TITLE AND SUBTITLE
Isotope Generated Electron Density in Silicon Carbide Direct Energy Converters

5a. CONTRACT NUMBER

5b. GRANT NUMBER

5c. PROGRAM ELEMENT NUMBER

6. AUTHOR(S)
Marc Litz and Kara Blaine

5d. PROJECT NUMBER

5e. TASK NUMBER

5f. WORK UNIT NUMBER

7. PERFORMING ORGANIZATION NAME(S) AND ADDRESS(ES)
U.S. Army Research Laboratory
ATTN: AMSRD-ARL-SE-DE
2800 Powder Mill Road
Adelphi, MD 20783-1197

8. PERFORMING ORGANIZATION REPORT NUMBER
ARL-TR-3964

9. SPONSORING/MONITORING AGENCY NAME(S) AND ADDRESS(ES)
U.S. Army Research Laboratory
2800 Powder Mill Road
Adelphi, MD 20783-1197

10. SPONSOR/MONITOR'S ACRONYM(S)

11. SPONSOR/MONITOR'S REPORT NUMBER(S)

12. DISTRIBUTION/AVAILABILITY STATEMENT
Approved for public release; distribution unlimited.

13. SUPPLEMENTARY NOTES

14. ABSTRACT
SiC has been investigated for use as a direct energy converter (DEC) for nuclear batteries. A solid-state model is being developed to calculate the electrical output of a diode into a resistively loaded circuit. This paper describes the use of a nuclear scattering code (MCNPX) to calculate the increased electron density that would be expected in a SiC material based on exposure to a Sr90 beta emitter. An incident beta (average 125 keV) generates on the order of 27k free electrons/cc per incident Sr90 electron. For each incident electron, and average of 9 keV is deposited in the SiC. The results of this effort will be fed into the Schottky device numerical model to calculate the predicted power from the device.

15. SUBJECT TERMS
DEC, SiC, nuclear battery

16. SECURITY CLASSIFICATION OF:			17. LIMITATION OF ABSTRACT	18. NUMBER OF PAGES	19a. NAME OF RESPONSIBLE PERSON
a. REPORT	b. ABSTRACT	c. THIS PAGE	SAR	22	Marc Litz
Unclassified	Unclassified	Unclassified			19b. TELEPHONE NUMBER (*Include area code*) 301-394-5556

Contents

List of Figures **iv**

1. Background **1**

2. Materials **2**

3. Numerical Simulations **3**

3.1 Geometry 3

3.2 Beta Source 4

4. Results **4**

5. Conclusions **9**

6. References **11**

Appendix A. MCNPX Input Deck **13**

Distribution List **15**

List of Figures

Figure 1. Schematic diagram of geometry of input deck of MCNPX. 4
Figure 2. Number density contour plot for (from left to right) (a) SiC, (b) Al, and (c) Si. The view is 5 mm by 0.15 mm, and the slice is 0.15 mm thick, representing 30-5 µm partial-layers. The binning is stored in such a way that each data point measures 250 µm by 8 µm by 150 µm. Closer inspection shows that the peak number density decreases by approximately 20% in each case. 5
Figure 3. Number density plot for (from top to bottom) (a) SiC, (b) Al, and (c) Si. The data is taken along the central line of the layers, where each point represents 250 µm by 8 µm by 150 µm. The data is shown with exponential fits. The point shown in the lower right of each plot is the exponential fit to the order of magnitude fall off from the starting point.... 6
Figure 4. Peak electron number density (a) data gathered from the Number Density Plots. The exponential fit was was extrapolated to zero, and the zero points, or starting points of the materials were plotted with respect to the density of the material. Electron range (b) data shows the point at which the density is 10% of the value at the surface of the material. 7
Figure 5. Energy spectrum of number density of electrons depositing energy into layers 1 through 3 of the 5 µm thick SiC layers. 8
Figure 6. Input beta spectrum from Strontium 90 is peaked at 125 keV. This spectrum is the input modeled in the MCNPX simulation..... 9

1. Background

Nuclear batteries can have a small but significant impact as a power source for long-lived sensors (*1-3*). For example, consider embedded sensors for bridges and foundations of large buildings where these sensors can provide information about the structural integrity (*4,5*). Unattended sensors for oceanic temperature measurement would need no maintenance during an increased operational lifetime. Unique opportunities are waiting for sensor applications that would benefit from keep-alive power lasting 30 years.

Chemical power sources can store the total energy required, but electrical leakage and deterioration stops them from sustaining the requisite power over long lifetimes. Nuclear batteries offer a unique source to fill the niche. Even though the energy storage density of nuclear isotopes is six orders of magnitude greater than that possible in chemical bonds, the stigma associated with nuclear materials will require careful design and thoughtful application. Sensors embedded in structures, providing information useful to monitor structural integrity may be just the application to overcome. The negatives often associated with nuclear applications.

MCNPX is a general-purpose Monte Carlo N-Particle code which supports 34 particle types, contains cross-section libraries, and includes the ability to use physics models for energies where tabular data are not available (*6*). MCNPX treats an arbitrary three-dimensional configuration of materials in geometric cells. Pointwise continuous-energy cross section data for scattering in materials are used. Source and tally structures with extensive statistical analysis of convergence are integral to the output parameters. Rapid convergence is enabled by a wide variety of variance reduction methods. MCNPX includes libraries for neutrons, photons, electrons, protons and photonuclear interactions. “Mesh” and “radiography” tallies are included for 2- and 3-dimensional imaging purposes. An auxiliary program, GRIDCONV, converts the mesh and radiography tally as well as standard metal-file results for viewing by independent graphics packages.

Monte Carlo algorithms calculate a statistically valid result of the most likely results of a set of operations (*7*). These algorithms are useful if you want to ask what will be the outcome of a series of events. This is particularly useful in complex series of molecular motions or a sequential series of events, as in photon scattering through a material. Each event has its own probability of occurrence. It can take days to run, in order to test as many events and outcomes as possible. These algorithms use random number generators to create the space for variety in the complexity and follow with variance reduction techniques to develop statistics that give guidance as to the value or weight of the answer. Credit for inventing the algorithm often goes to Stanislaw Ulam. Unlike Monte Carlo simulation, deterministic transport methods require that the phase-space be discretized in space, energy and angle, introducing a substantial degree of complication in terms of algorithm development, problem set-up, and requires a significant

amount of computer memory in order to store the spatial, angular and energy dependent flux information. The large demand placed on computer memory by deterministic transport codes has limited their use. However, with the rapid increase in computer processing power, memory capacity, and reduction in unit cost, three-dimensional, time-independent, deterministic transport codes are now becoming available as production codes (*8*).

This paper describes the MCNPX simulations developed to determine the free electron density generated in bulk SiC layers. The β-particle source stimulation modeled in the numerical simulation is the spectrum of β emitted from the Sr90 isotope. The electron density gradient calculated in SiC is then used as initial conditions for a drift-diffusion numerical model of a Schottky diode.

Section 1 provides the motivation for our efforts and discusses some of the applications that will benefit from the effort. Section 2 discusses SiC and the devices developed for this application. Section 3 details the geometry model input to the monte-carlo code. Sections 4 details the significant results and section 5 provides conclusions and impact of this part of the larger effort.

2. Materials

Silicon Carbide (SiC) is a robust radiation-hard solid-state material that can be fabricated into many device formats. For these reasons it is worth pursuing as a direct energy converter (DEC) from radiation (alphas, betas, or gammas) into free electrons that can be used as a source of electrical current. A parametric study of both materials and device geometry is underway. Materials under investigation include silicon (Si -2.3 g/cc), SiC (3.2 g/cc), gallium nitride (GaN - 6.15 g/cc), and CVD Diamond (3.52 g/cc). Device geometries are not identical for all materials, however, PIN and Schottky geometries have been acquired. Both Si and SiC Schottky diodes are fabricated at the Army Research Laboratory. The diodes have been exposed to betas emitted from Strontium-90, with the voltage across the diode measured during controlled experiments. The irradiation of these devices from strontium-90 will be the focus of this paper. A more complete review of PIN diode structures will be part of future efforts.

We composed the results of numerical simulations on Al, Si and SiC. While the Si and SiC simulations model devices were built and measured in experiments, the purpose of the aluminum (Al – 2.7 g/cc) is 1) to compare to the Si and SiC, and 2) serve as a reference material for electron range results. Tables of electron losses have been tabulated for a variety of materials including Al (*9*). The Berger and Seltzer report includes tables of range constants (g/cm^2) as a function of monochromatic beta energy. The incoming beta energy used as a comparison in our calculations is 150 keV betas, which is a good comparison for our 125 keV (average) beta

spectrum used in the MCNPX calculations. The range constant supplied in section 3.2 (*9*) must be multiplied by the density of the material used. The density of Al is shown in equation 1.

$$3.64\times10^{-2}\,\frac{g}{cm^2}\cdot\frac{1}{2.7\,g/cm^3}=1.3\times10^{-2}\,cm=130\mu m \qquad (1)$$

The range of the aluminum hit by the constant energy 150 keV betas is shown to be 130 μm, as shown in equation 1, above, which is a good comparison to the 150 μm deep model used, which will be described in more detail in section 3.1.

3. Numerical Simulations

3.1 Geometry

The MCNPX input deck that defines the geometry used for this study (see appendix A) created thirty rectangular parallelepipeds of material layers in a row, located 1 mm from a 0.5 mm in diameter beta source (see figure 1). The physical diode package, used in the experiments, measures 5 mm by 5 mm by 0.5 mm. However, our interest was to see the number of electrons generated in the top-most layers of Schottky diodes, which have a depletion layer of approximately 5 μm thick. Therefore, the layers used in the input deck measured 5 mm by 5 mm in the plane perpendicular to the beta source and 5 μm deep. All together, the thickness of the SiC totaled 150 μm to ensure a complete stopping range for the betas.

It is essential to note that the diode interaction with the electrical circuit cannot be simulated within the MCNPX code. Instead, we are only modeling the SiC material and attempting to calculate how many free-electrons are being generated within as a function of depth in the material. A separate numerical solid-state code will be used in an additional study to analyze the electrical response of the diode with respect to an external circuit. This will be discussed in subsequent papers.

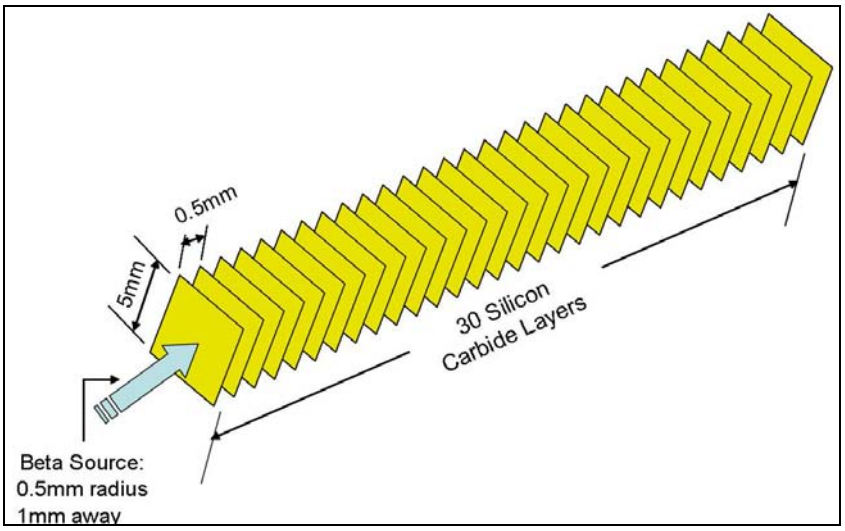

Figure 1. Schematic diagram of geometry of input deck of MCNPX.

3.2 Beta Source

The beta source coded into the MCNPX input deck (see appendix A) is an attempt to model a strontium-90 (Sr-90) beta emitter. There are several flaws with the MCNPX approximation, which are small, but necessary to recognize. Strontium-90 emits a beta spectrum up to 547 keV. However, the MCNPX input deck was simplified to an input spectrum of 500 keV, which peaks at 125 keV based on previous calculations. This was not a terrible assumption considering that the spectrum of electron energies emitted from the isotope is usually peaked at one third the maximum energy of the emitted beta (*10*). The beta input spectrum used to simulate the Sr90 isotope is shown in figure 6. Furthermore, when low energy electrons enter the material, fewer additional electrons are generated, though the energy of the electrons may be more suitable to be captured by the depletion region and converted into usable power in a circuit.

4. Results

Contour plots of electron number density (#/cc), shown in figure 2, were generated for each of the three materials being evaluated: SiC, Al, and Si. The calculation using MCNPX gives results of energy deposited with units of MeV/g. The number density is calculated from these original results by a) multiplying by material density and b) dividing by the average particle energy (125 keV). The number density data was calcualted by recording MCNPX mesh diagnostic over a volume that spanned 5 mm by 0.15 mm by 0.15 mm. The SiC layer volume modeled in the MCNPX input deck occupies a total of 5 mm by 5 mm by 0.15 mm. In order to get a number density at the center of the beam, the mesh diagnostic was implemented to

calculate the energy deposited over a much smaller volume (at the beam center) than the entire layer. The binning of the mesh data cell was defined to be 250 µm by 8 µm by 150 µm. By taking a smaller mesh size, a more accurate description was obtained. The results of the contour plots show that the number density at the center of the beam is 27 k electrons/cc/incident electron.

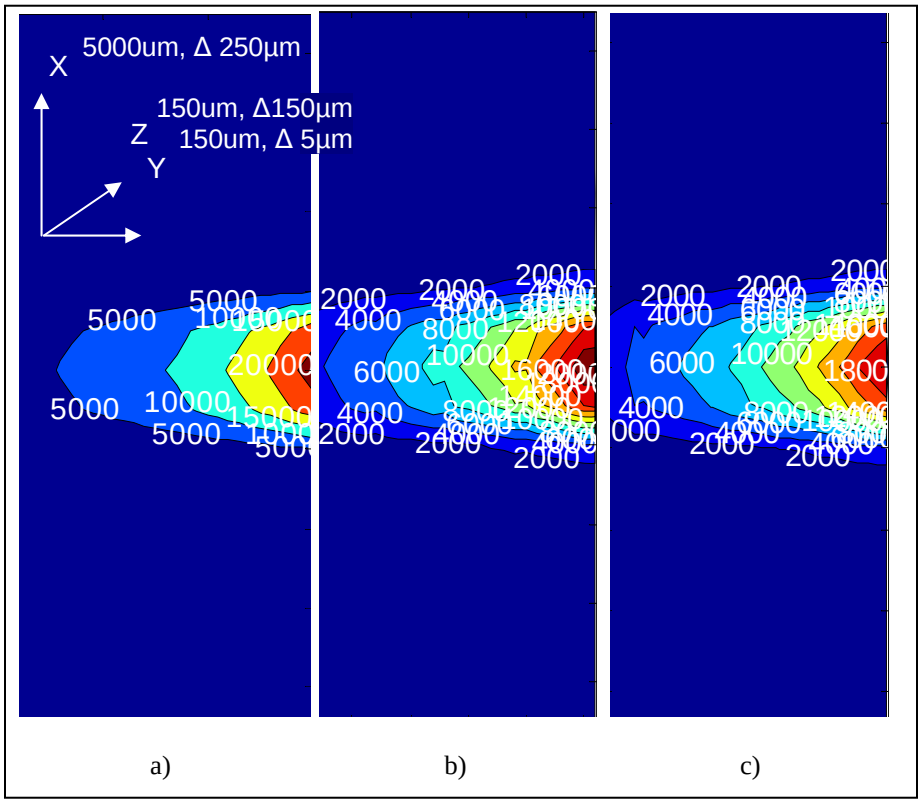

Figure 2. Number density contour plot for (from left to right) (a) SiC, (b) Al, and (c) Si. The view is 5 mm by 0.15 mm, and the slice is 0.15 mm thick, representing 30-5 µm partial-layers. The binning is stored in such a way that each data point measures 250 µm by 8 µm by 150 µm. Closer inspection shows that the peak number density decreases by approximately 20% in each case.

Number density plots (figure 3) show a 1-dimensional horizontal cut across the contour plots of figure 2. They curves show more quantitatively, the number density values along the center-line (beam-line) in 1-dimension, compared to what is pictured in 2-D in the contour plots of figure 2. With the addition of a trend line to each data set, the number density is shown to decrease exponentially as electrons propagate the layers of SiC. Variation from the line may result from poor statistics, which, though satisfactory, could be improved with more histories numerically calculated (and longer run times). The statistical result of the mesh calculation is well below 10% which provides a high degree of certainty.

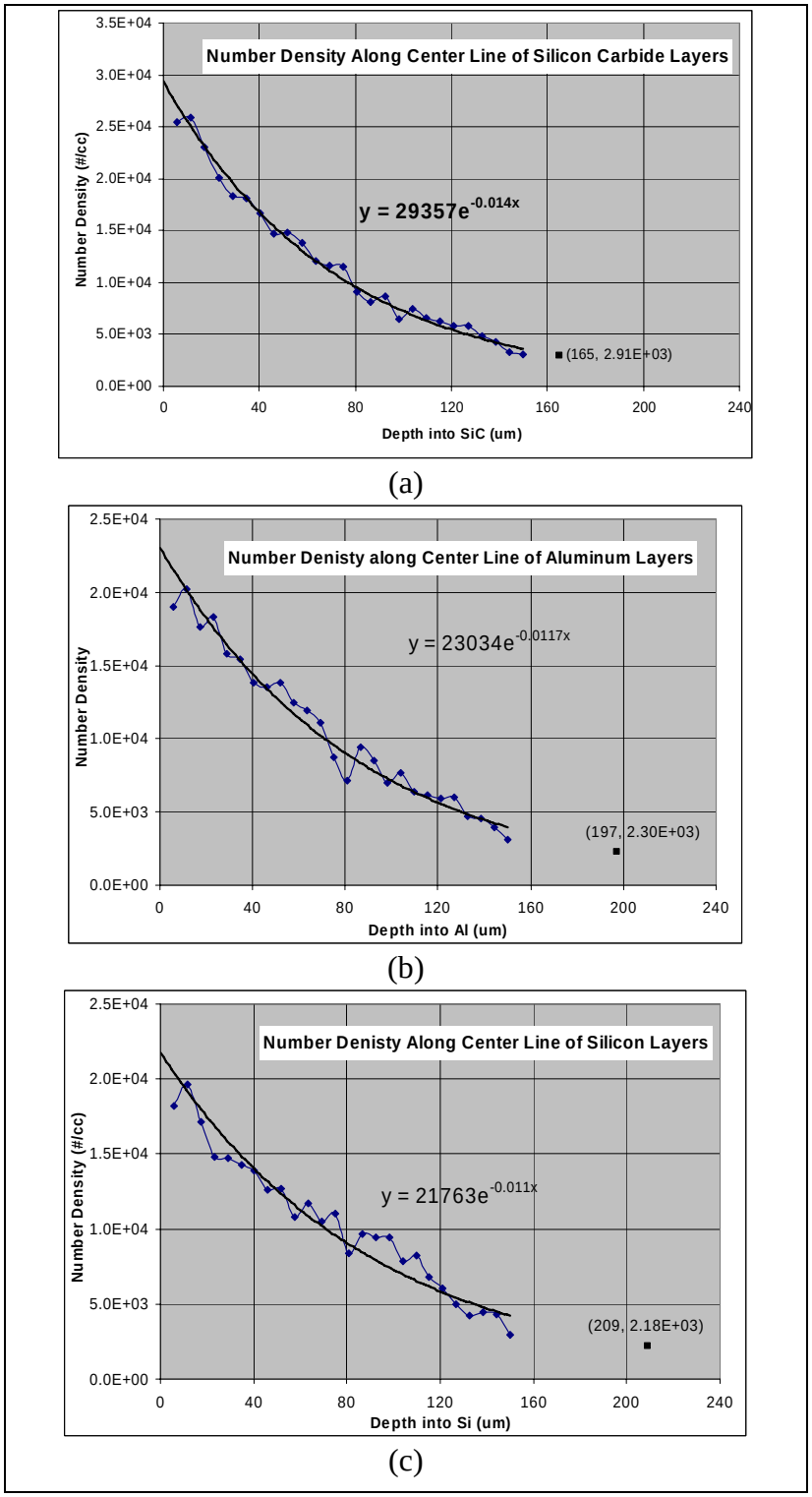

Figure 3. Number density plot for (from top to bottom) (a) SiC, (b) Al, and (c) Si. The data is taken along the central line of the layers, where each point represents 250 µm by 8 µm by 150 µm. The data is shown with exponential fits. The point shown in the lower right of each plot is the exponential fit to the order of magnitude fall off from the starting point.

We expected that the number of free electrons generated in the materials would be correlated to material density. They are not, however, linearly dependent on material density. With only three data points to compare, it is left for a future study, to better understand this result. One way to understand this discrepancy, is that not only was the material density changing, but so were the atomic scatterers. The density varied during the three calculations from 2.3, 2.7, and 3.2 g/cc, while the atomic number of the materials also changed from Si(atomic mass 28.1), Al(atomic mass 26.9), and SiC. A linear approximation is still attempted to fit the density of free electrons generated by the Sr90 betas with changing density of the DEC material. This linear fit to the data is shown below in figure 4.

The electron range of each of the three DEC materials is plotted (figure 4) as a function of the DEC material density. The electron range here is defined as 10% of initial number density at the surface. Before extrapolation, all the materials looked like they would have a similar fall off point, though closer inspection revealed that the number density has a linear relationship with respect to material density, just as the peak number density does. However, more data would be needed for a better evaluation.

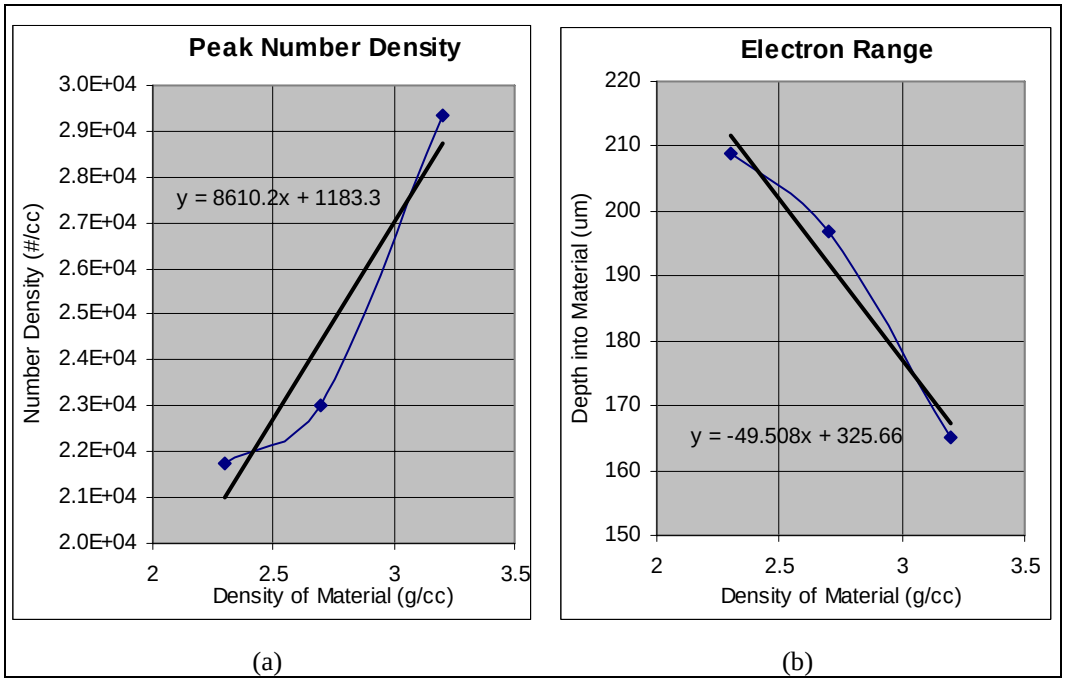

Figure 4. Peak electron number density (a) data gathered from the Number Density Plots. The exponential fit was was extrapolated to zero, and the zero points, or starting points of the materials were plotted with respect to the density of the material. Electron range (b) data shows the point at which the density is 10% of the value at the surface of the material.

The spectrum of the electrons depositing energy in a layer is shown in figure 5. This graph clearly shows that the lower energy electrons are responsible for depositing most of the energy in the system. The spectrum shown is unlike the shape of the input Sr90 spectrum. The beta spectrum bombarding the SiC layers is shown in figure 6. The comparison of input beta

spectrum, and spectrum of electrons depositing energy in the material shows that the higher energy betas tend to travel through the material without leaving much energy behind. This would lead us to believe that the scattered, lower-energy (<100 keV) electrons are more significant in providing power to an external circuit.

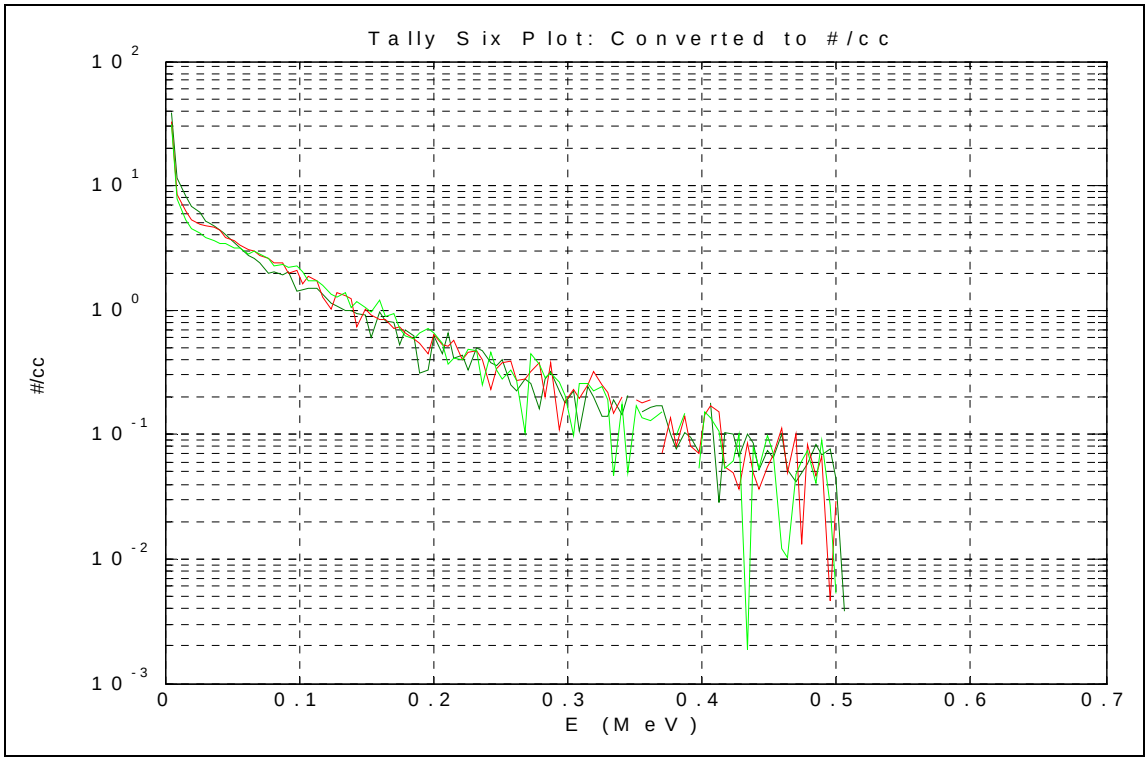

Figure 5. Energy spectrum of number density of electrons depositing energy into layers 1 through 3 of the 5 µm thick SiC layers.

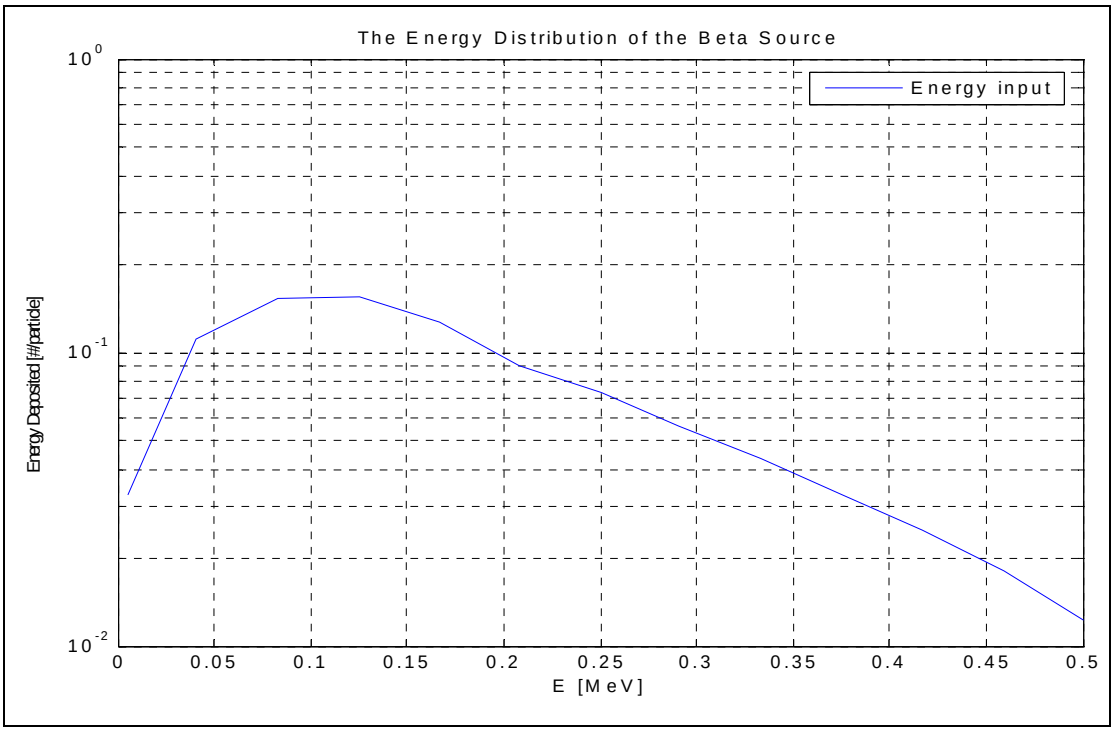

Figure 6. Input beta spectrum from Strontium 90 is peaked at 125 keV. This spectrum is the input modeled in the MCNPX simulation.

5. Conclusions

The number density result calculated in MCNPX is the number of electrons generated for each incident electron. The Sr90 source used in our experiments is physically located at NSWC-Carderock. It has an activity of 7mCi. This corresponds to 25e7 beta emissions per second (Bq). The resulting number density of electrons generated as a result of our experimental setup is then calculated in the SiC converter experiments to be 675e10/cc/sec.

The range for betas emitted from Strontium 90 has been modeled using MCNPX. The results show that 150 μm of SiC stops all electrons emitted. A parametric study of target material was performed using MCNPX. Input decks for this numerical investigation differ only by material (Al, Si, and SiC) and their corresponding naturally occurring density. These results compare well with values generated by Berger and Selter (*8*) in which they tabulated the values of stopping range in Al, Si and Cu.

Diagnostics available in the MCNPX simulations were compared for consistency. Surface flux results (tally 2) compare well with volume flux results (tally 4), in the limit as the thickness of the volume decreased to a surface.

When calculating the energy deposited in the material, tally 6 generates a result over a complete cell. When a more localized or discretized value is required (i.e., the value at the center of the beam), using the mesh command and identifying smaller effective volume regions works well and compares accurately to the averaged value over the larger volume of the cell. The value calculated for energy deposited per incident electron per gram of material is 22.6 MeV/g. The layer dimension is 5 mm x 5 mm x 5 μm, or 1.25e-4 cc. The density of SiC is 3.2 g/cc corresponding to a layer mass of 4e-4 g. The resulting energy deposited is 9.04 keV. This represents 7% of the peak incident-electron-energy (125 keV), deposited in a 5 um layer of SiC.

In a prototype isotope battery design, foils will be sandwiched in-between two SiC DEC devices. In order to better understand the efficiency that would be expected from an isotope foil above the SiC DEC layer, we performed a broad beam simulation. The incident beam radius was varied [0.5, 1, 2, 5 mm]. Beams diameters, less than 2 mm, generated electron showers completely within the 5 mm side-length of the devices under test. The energy deposited in the first 5 μm layer was calculated to be 22.6 MeV/g. 2.26% of the incident energy is deposited in the first layer. This result is identical to the previous pencil beam simulations.

These nuclear scattering calculations do not take into account the electrical circuit properties of a diode (i.e., source impedance feeding a load impedance). The numerical simulations described above are meant to determine an initial electron density, or density of carriers for initial conditions into a circuit-based model. The initial conditions are used in a study, already underway, to model the drift and diffusion in diode structures. The results will be reported in our next technical report of the investigation.

The follow-on circuit modeling is expected to provide current and voltage numerical results and insight into the electron flow within the semiconductor materials that convert the emitted-beta energy into electrical current for a long-lived power source. The results of the circuit models being developed will be compared to measurements. With electron density initial conditions (the result of this investigation), a circuit model, and measurements in-hand, an optimized DEC for a nuclear battery design is expected as a result in the near future.

6. References

1. Blanchard, James P. Stretching the Boundaries of Nuclear Technology. The Bridge 32.4 (2002): 29-34.
2. Ahearne, John F. The Future of Nuclear Energy. Editorial. The Bridge 31.3 (2001).
3. Bugliarello, George. Our Energy Future. Editorial. The Bridge 32.2: 3-4.
4. Lal, Amit; Blanchard, James. The Daintiest Dynamos. *IEEE Spectrum* **Sept. 2004**, 36-41.
5. Lal, A.; Blanchard, James. By Harvesting Energy From Radioactive Specks, Nuclear Micrbatteries Could Power Tomorrow's Microelectromechanical Marvels-And May Be Your Cellphone Too. *IEEE Spectrum* **September 2004**, 36-41.
6. Briesmeister, J. F. ed. MCNP™-A General Monte Carlo N-Particle Transport Code, LA-12625-M, Version 4B (March 1997).
7. Metropolis, Nicholas; Ulam, Stanislaw. The Monte Carlo method. *Journal of the American Statistical Association* **1949**, *44* (247), 335-341.
8. Kodeli, I. Progress on Computational Tools for 3D Sensitivity and Uncertainty Analsyis. OCED-NEA Seminar on 3D Deterministic Radiation Transport Computer Programs Features, Applications and Perspectives, Paris (2-3 Dec. 1996).
9. Berger, Martin J.; Seltzer, Stephen M. Tables of Energy Losses and Ranges of Electrons and Positrons. National Aeronautics and Space Administration. Scientific and Technical Information Division, 1964, p 64.
10. Cross, W. G.; Ing, H.; Freedman, N. A short atlas of beta-ray spectra. *Phys. Med. Biol.*, *28* (11), 1251-1260.

Other Related Manuscripts:

11. Nickel: Human Health Fact Sheet. Argonne National Laboratory, EVS, August 2005.
12. Energy Conversion Vol 13, pp. 117-127, Pergamon Press, 1973
13. Silicon CarbideAlphavoltaic Battery, Rybicki, George, 25th PVSC, May 13-17, 1996, Washington, D.C.
14. Si, H.; Lal, A.; Blanchard, J.; Henderson, D. Self-reciprocating radioisotope-powered cantilever. *J. Appl. Phys.* **2002**, *92* (2), 1122-7.
15. Pfann, W. G.; van Roosbroeck, V. Radioactive and Photoelectric p-n Junction Power Sources. *J. Appl. Phys.* **1954**, *25* (11), 1422-34.

16. Olsen, L. C. Betavoltaic energy Conversion. *Energy Conversion* **1973**, *13*, 117-27.

17. Spitsyn, A. B.; Prelas, M. A.; Tompson, Robert V.; Ghosh, T. K. Impurity Removal from 4-H SIC using reversed Field Enhanced Diffusion with Optical Activation, Accepted for Publication in the Journal of Wide Band-Gap Materials, May 2002.

18. Physics of radiation Effects in Crystals, eds. R. A. Johnson and A. N. Orlov, North-Holland, New York, 1986.

19. Yamaguchi, M.; Yang, M.; Imaizumi, M.; Matsuda, S.; Kawasaki, O.; Hisamatsu, T. Type conversion in irradiated silicon diodes. *Appl. Phys. Lett.* **1997**, *70*, 2165.

20. Prelas, M.; Charlson, E. J.; Meese, J.; Popovici, G.; Stacy, T. Diamond Photovoltaic Energy Conversion, Second International Conference on the Application of Diamond Films and Related Materials, Editors M. Yoshikawa, M. Murakawa, Y. Tzeng and W. A. Yarbrough, MY Tokyo, Pages 5-12 (1993).

21. Prelas, M.; Ghosh T.; Tompson, R. Direct Conversion of Radioisotope Energy to Electricity, Year 3 Report for DOE contract, DE FG07-001D13927, August 2003.

22. Brown, P. M. Betavoltaic batteries. *Journal of New Energy* **2001**, *5* (4), 35-42.

23. Brown, P. Betavoltaic batteries. *New England News* **1999**, *6* (11), 2-3.

Appendix A. MCNPX Input Deck

The input deck shown below is one of the series of numerical simulations evaluated.

sicm3

```
Model of Silicon Carbide with Sr source
c (MCNPX scaled in cm)
c
c ---------------------------------------------------------
c This is a model of the way electrons would be generated
c in the SiC after being hit by electrons from a strontium source.
c ---------------------------------------------------------
c
c +--------------------------------------------------------+
c |                                                        |
c |                    Cell Cards                          |
c |                                                        |
c +--------------------------------------------------------+
c # mat   density   surface        data
c SiC
  1  3    -3.2       -1          imp:e 1  u=1    $SiC layer closest to source
  2  3    -3.2       -2          imp:e 1  u=1    $2nd SiC layer
  3  3    -3.2       -3          imp:e 1  u=1    $3rd SiC layer
  4  3    -3.2       -4          imp:e 1  u=1    $4th SiC layer
  5  3    -3.2       -5          imp:e 1  u=1    $5th SiC layer
  6  3    -3.2       -6          imp:e 1  u=1    $6th SiC layer
  7  3    -3.2       -7          imp:e 1  u=1    $7th SiC layer
  8  3    -3.2       -8          imp:e 1  u=1    $8th SiC layer
  9  3    -3.2       -9          imp:e 1  u=1    $9th SiC layer
 10  3    -3.2       -10          imp:e 1  u=1    $10th SiC layer
 11  3    -3.2       -11          imp:e 1  u=1    $11th SiC layer
 12  3    -3.2       -12          imp:e 1  u=1    $12th SiC layer
 13  3    -3.2       -13          imp:e 1  u=1    $13th SiC layer
 14  3    -3.2       -14          imp:e 1  u=1    $14th SiC layer
 15  3    -3.2       -15          imp:e 1  u=1    $15th SiC layer
 16  3    -3.2       -16          imp:e 1  u=1    $16th SiC layer
 17  3    -3.2       -17          imp:e 1  u=1    $17th SiC layer
 18  3    -3.2       -18          imp:e 1  u=1    $18th SiC layer
 19  3    -3.2       -19          imp:e 1  u=1    $19th SiC layer
 20  3    -3.2       -20          imp:e 1  u=1    $20th SiC layer
 21  3    -3.2       -21          imp:e 1  u=1    $21th SiC layer
 22  3    -3.2       -22          imp:e 1  u=1    $22th SiC layer
 23  3    -3.2       -23          imp:e 1  u=1    $23th SiC layer
 24  3    -3.2       -24          imp:e 1  u=1    $24th SiC layer
 25  3    -3.2       -25          imp:e 1  u=1    $25th SiC layer
 26  3    -3.2       -26          imp:e 1  u=1    $26th SiC layer
 27  3    -3.2       -27          imp:e 1  u=1    $27th SiC layer
 28  3    -3.2       -28          imp:e 1  u=1    $28th SiC layer
 29  3    -3.2       -29          imp:e 1  u=1    $29th SiC layer
 30  3    -3.2       -30          imp:e 1  u=1    $30th SiC layer
c
c air encasing
 31  2    -0.00129   -31 1 2 3 4 5 6 7 8 9 10 11 12 13 14 15 16 17 18 19 &
     20 21 22 23 24 25 26 27 28 29 30  imp:e 1  u=1
c
 32  0   1 2 3 4 5 6 7 8 9 10 11 12 13 14 15 16 17    &
       18 19 20 21 22 23 24 25 26 27 28 29 30       imp:e 1  u=1
 33  0               31          imp:e 1 u=1
c room
 34  2    -0.00129   -32          imp:e 1 fill=1
 35  0               32          imp:e 0        $outside world

c +--------------------------------------------------------+
c |                                                        |
c |                    Surface Cards                       |
c |                                                        |
c +--------------------------------------------------------+
c # type params
c SiC
 1   rpp  708.75 709.25  493.9995 494      117.25 117.75   $SiC layer closest to source
 2   rpp  708.75 709.25  493.9990 493.9995  117.25 117.75   $2nd SiC layer
 3   rpp  708.75 709.25  493.9985 493.9990  117.25 117.75   $3rd SiC layer
 4   rpp  708.75 709.25  493.9980 493.9985  117.25 117.75   $4th SiC layer
 5   rpp  708.75 709.25  493.9975 493.9980  117.25 117.75   $5th SiC layer
 6   rpp  708.75 709.25  493.9970 493.9975  117.25 117.75   $6th SiC layer
 7   rpp  708.75 709.25  493.9965 493.9970  117.25 117.75   $7th SiC layer
 8   rpp  708.75 709.25  493.9960 493.9965  117.25 117.75   $8th SiC layer
 9   rpp  708.75 709.25  493.9955 493.9960  117.25 117.75   $9th SiC layer
10   rpp  708.75 709.25  493.9950 493.9955  117.25 117.75   $10th SiC layer
11   rpp  708.75 709.25  493.9945 493.9950  117.25 117.75   $11th SiC layer
12   rpp  708.75 709.25  493.9940 493.9945  117.25 117.75   $12th SiC layer
13   rpp  708.75 709.25  493.9935 493.9940  117.25 117.75   $13th SiC layer
14   rpp  708.75 709.25  493.9930 493.9935  117.25 117.75   $14th SiC layer
15   rpp  708.75 709.25  493.9925 493.9930  117.25 117.75   $15th SiC layer
16   rpp  708.75 709.25  493.9920 493.9925  117.25 117.75   $16th SiC layer
17   rpp  708.75 709.25  493.9915 493.9920  117.25 117.75   $17th SiC layer
18   rpp  708.75 709.25  493.9910 493.9915  117.25 117.75   $18th SiC layer
19   rpp  708.75 709.25  493.9905 493.9910  117.25 117.75   $19th SiC layer
20   rpp  708.75 709.25  493.9900 493.9905  117.25 117.75   $20th SiC layer
21   rpp  708.75 709.25  493.9895 493.9900  117.25 117.75   $21th SiC layer
22   rpp  708.75 709.25  493.9890 493.9895  117.25 117.75   $22th SiC layer
23   rpp  708.75 709.25  493.9885 493.9890  117.25 117.75   $23th SiC layer
24   rpp  708.75 709.25  493.9880 493.9885  117.25 117.75   $24th SiC layer
25   rpp  708.75 709.25  493.9875 493.9880  117.25 117.75   $25th SiC layer
26   rpp  708.75 709.25  493.9870 493.9875  117.25 117.75   $26th SiC layer
27   rpp  708.75 709.25  493.9865 493.9870  117.25 117.75   $27th SiC layer
28   rpp  708.75 709.25  493.9860 493.9865  117.25 117.75   $28th SiC layer
29   rpp  708.75 709.25  493.9855 493.9860  117.25 117.75   $29th SiC layer
30   rpp  708.75 709.25  493.9850 493.9855  117.25 117.75   $30th SiC layer
c lead block to encase silicon carbide
31   rpp  708.5  709.5   493.850 494     117 118
c room dimensions
32   rpp  0 1419  0 1984  0 466
c +--------------------------------------------------------+
c |                                                        |
c |                    Material Cards                      |
c |                                                        |
c +--------------------------------------------------------+
c m# isotope     percent   &
c  m1  82000       1.0       $lead 11.34 g/cc
   m2   8016        .3       &
        7014        .7       $air 0.00129 g/cc
   m3   6012        .43      &
       14028        .57      $SiC 3.2 g/cc
c  m4  14028       1.0       $Si  2.3 g/cc
c  m13  6012       1.0       $C   2.3 g/cc
c  m5  90000       1.0       $Sr
c
c +--------------------------------------------------------+
c |                                                        |
c |                    Source Definition                   |
c |                                                       |
c +--------------------------------------------------------+
sdef          &
    dir=1     &
    erg= d2     &
    vec=0 -1 0 &
    par=e      &
    rad=d1     &
    pos=709 497 117.5
c
 si1 0 .05
 sp1 -21
c
c energy distribution taken from  now strontium (old: 280kv-8ma-12may-aft.spe)
 si2 0.000916 0.00549 0.0412 0.0833 0.125 0.167 0.208 0.25 0.291 0.333 &
     0.375 0.417 0.459 0.5
 sp2 0        1000    3405   4692   4768  3900  2775  2234  1725  1331  &
      1007  764  556   378
c
c  si3 h .707 1
c  sp3 d 0 1
c
```

```
c +-------------------------------------------------------+
c |                                                       |
c |                    Data Cards                         |
c |                                                       |
c +-------------------------------------------------------+
mode e
nps 10000     $10Mh~9hrs
c
c +-------------------------------------------------------+
c |                                                       |
c |                    Tallies                            |
c |                                                       |
c +-------------------------------------------------------+
c
c
fc2 test
f2:e 1.3
e2 0 98i .51
c
c fc4 electron flux averaged over the cell in particles/cm^2
c f4:e 1 2 3
c e4 0 98i .51
c
c
c this tally may not work (or be correct) because it is with electrons
c fc6 electron energy deposition averaged over the cell in MeV/g
c f6:e 1 2 3
c e6 0 98i .51
c
c fc8 electron energy deposition in MeV
c *f8:e 1 2 3
c e8 0 1e-5 97i .51
c
c +-------------------------------------------------------+
c |                                                       |
c |                    Mesh                               |
c |                                                       |
c +-------------------------------------------------------+
c
tmesh
c
c (a)radial meshes (b)zaxis(symmetry) (c)angles counterclockwise
c
c  flux=#/cm2     $dose=rem/hr    $pedep=MeV/cm3
c
c flux: flux
c pedep: total energy deposition/unit vol
c dose: dose over cross planes
c
rmesh1:e  flux pedep popul dose
c layer 1 SiC
cora1    708.75   18i  709.25
corb1    493.9995      494
corc1    117.25   18i  117.75
c
rmesh21:e  flux pedep popul dose
c layer 1 SiC
cora21   708.75   18i  709.25
corb21   493.9995 18i  494
corc21   117.25        117.75
c
rmesh31:e  flux pedep popul dose
c layer 1 SiC
cora31   708.75        709.25
corb31   493.9995 18i  494
corc31   117.25   18i  117.75
c
c
rmesh41:e  flux pedep popul dose
c layer 2 SiC
cora41    708.75   18i  709.25
corb41    493.999       493.9995
corc41    117.25   18i  117.75
c
rmesh51:e  flux pedep popul dose
c layer 2 SiC
cora51   708.75   18i  709.25
corb51   493.999  18i  493.9995
corc51   117.25        117.75
c
rmesh61:e  flux pedep popul dose
c layer 2 SiC
cora61   708.75        709.25
corb61   493.999  18i  493.9995
corc61   117.25   18i  117.75
c
c
rmesh71:e  flux pedep popul dose
c layer 3 SiC
cora71    708.75   18i  709.25
corb71    493.9985      493.999
corc71    117.25   18i  117.75
c
rmesh81:e  flux pedep popul dose
c layer 3 SiC
cora81   708.75   18i  709.25
corb81   493.9985 18i  493.999
corc81   117.25        117.75
c
rmesh91:e  flux pedep popul dose
c layer 3 SiC
cora91   708.75        709.25
corb91   493.9985 18i  493.999
corc91   117.25   18i  117.75
c
c
rmesh101:e  flux pedep popul dose
c all SiC layers (30)
cora101   708.75   18i  709.25
corb101   493.985  25i  494
corc101   117.4925      117.5075
c
endmd
```

Distribution List

ADMNSTR
DEFNS TECHL INFO CTR
ATTN DTIC-OCP (ELECTRONIC COPY)
8725 JOHN J KINGMAN RD STE 0944
FT BELVOIR VA 22060-6218

DARPA
ATTN IXO S WELBY
3701 N FAIRFAX DR
ARLINGTON VA 22203-1714

OFC OF THE SECY OF DEFNS
ATTN ODDRE (R&AT)
THE PENTAGON
WASHINGTON DC 20301-3080

US ARMY TRADOC
BATTLE LAB INTEGRATION & TECHL DIRCTRT
ATTN ATCD-B
10 WHISTLER LANE
FT MONROE VA 23651-5850

SMC/GPA
2420 VELA WAY STE 1866
EL SEGUNDO CA 90245-4659

COMMANDING GENERAL
US ARMY AVN & MIS CMND
ATTN AMSAM-RD W C MCCORKLE
REDSTONE ARSENAL AL 35898-5000

US ARMY INFO SYS ENGRG CMND
ATTN AMSEL-IE-TD F JENIA
FT HUACHUCA AZ 85613-5300

US ARMY SIMULATION TRAIN & INSTRMNTN CMND
ATTN AMSTI-CG M MACEDONIA
12350 RESEARCH PARKWAY
ORLANDO FL 32826-3726

US GOVERNMENT PRINT OFF
DEPOSITORY RECEIVING SECTION
ATTN MAIL STOP IDAD J TATE
732 NORTH CAPITOL ST., NW
WASHINGTON DC 20402

US ARMY RSRCH LAB
ATTN AMSRD-ARL-CI-OK-TP
TECHL LIB T LANDFRIED (2 COPIES)
BLDG 4600
ABERDEEN PROVING GROUND MD
21005-5066

DIRECTOR
US ARMY RSRCH LAB
ATTN AMSRD-ARL-RO-EV
W D BACH
PO BOX 12211
RESEARCH TRIANGLE PARK NC 27709

ECOPULSE INC
7844 VERVAIN CT
SPRINGFIELD VA 22150

US ARMY RSRCH LAB
ATTN AMSRD-ARL-D J M MILLER
ATTN AMSRD-ARL-CI-OK-T
TECHL PUB (2 COPIES)
ATTN AMSRD-ARL-CI-OK-TL
TECHL LIB (2 COPIES)
ATTN AMSRD-ARL-SE-DE
M LITZ (10 COPIES)
ATTN AMSRD-ARL-SE-DE
K BLAINE (10 COPIES)
ATTN AMSRD-ARL-SE-DB
G MERKEL
ATTN IMNE-ALC-IMS
MAIL & RECORDS MGMT
ADELPHI MD 20783-1197

INTENTIONALLY LEFT BLANK.